Spectral Measurements and Other Features of Separating Turbulent Flows

Roger L. Simpson,* Naval K. Agarwal,† K. A. Nagabushana,‡ and S. Olcmen§
Virginia Polytechnic Institute and State University, Blacksburg, Virginia

Measurements from two strong adverse-pressure-gradient separating turbulent boundary-layer flows are presented. Detailed study of spectra shows that the flow variables $\phi_{uu}(k_1\delta)/-\overline{uv}_{max}$ vs $k_1\delta$ form a set of scaling parameters for streamwise velocity fluctuation power spectra from these and other adverse pressure gradient flows. The backflow mean velocity profile scales on the maximum negative mean velocity U_N and its distance from the wall N. In the mean backflow region, there appears to be a semilogarithmic region in profiles of the streamwise fluctuating velocity component, u', which spreads over a definite range of y/δ.

Nomenclature

A_0 = universal constant for inverse power law in u spectra
C_f = skin friction coefficient, Eq. (6)
C_p = pressure coefficient, Eq. (1)
f = frequency, Hz
H = shape factor, $= \delta^*/\theta$
K_0 = universal constant for $-5/3$ power law in u spectra
k_1 = wavenumber, $= 2\pi f/U$
l = spectral length scale
M = distance of maximum $-\overline{uv}$ from the wall
N = distance of maximum mean negative velocity from the wall
P = pressure
$-\overline{\rho uv}$ = Reynolds shear stress
Re_θ = Reynolds number based on the momentum thickness
U_N = maximum negative velocity
U_w = wall region scaling parameter for velocity
U_τ = frictional velocity, $\sqrt{\tau_w/\rho}$
U_∞ = local freestream velocity
U^+ = nondimensional velocity $= U/U_\tau$
$\overline{u^2}$ = mean square of longitudinal velocity fluctuation, u
u' = rms of longitudinal velocity fluctuation, $= \sqrt{\overline{u^2}}$
V = normal component of local mean flow velocity
$\overline{v^2}$ = mean square of normal velocity fluctuation, v
v' = rms of normal velocity fluctuation, $= \sqrt{\overline{v^2}}$
x = streamwise distance from the leading edge
y = normal distance from the wall
y_w = wall region scaling parameter for distance
y^+ = a Reynolds number, $= yU_\tau/v$
β = flow incidence angle to the cross-wire bisector
γ_{pu} = downstream-upstream intermittency
δ = boundary-layer thickness, y where $U/U_\infty = 0.99$
δ^* = displacement thickness
ε = turbulence energy dissipation rate
θ = momentum thickness
κ = von Kármán constant, $= 0.41$
ρ = density
τ_w = wall shearing stress
ϕ_{uu} = power spectrum of u velocity component,

$$\overline{u^2} = \int_0^\infty \phi_{uu}(k_1\ell)\,\mathrm{d}(k_1\ell)$$

I. Introduction

As a turbulent boundary layer undergoes an adverse pressure gradient, the flow near the wall decelerates until some backflow first occurs (Fig. 1) at incipient detachment (ID), defined as the near-wall location where the fraction of time that the flow moves downstream, γ_{pu}, is 0.99. Large eddies, which bring outer region momentum toward the wall, supply some downstream flow. These large eddies grow rapidly in all directions and agglomerate with one another to decrease the average frequency of passage as detachment ($\bar{\tau}_w = 0$; $\gamma_{pu} = 0.5$) is approached. Substantial pressure gradient relief begins near intermittent transitory detachment (ITD) defined as $\gamma_{pu} = 0.8$ near the wall.

Several common experimentally observed features for all types of separating and reattaching flows are discussed by Simpson.[1,2] In the vicinity of detachment, the turbulence intensities become the largest in the middle of the shear layer. Lower $-\overline{uv}/u'v'$ correlation coefficients occur than for attached flows. Large-scale structures pair to form larger structures that pass downstream at lower frequencies. Mean velocity profiles look similar to those for mixing layers, except near the wall where backflow occurs. The mean backflow profile scales on the maximum mean backflow velocity and its distance from the wall. The backflow is strongly controlled by the maximum shear stress within the flow. The traditional semilogarithmic law-of-the-wall velocity profile does not describe the backflow for low-velocity backflows with negligible Reynolds shearing stresses.

Experimental results are described here for two nominally two-dimensional separating turbulent boundary layers for airfoil-type pressure distribution flows, which detach and reattach some distance downstream soon after detachment. Upstream of separation, single and cross-wire hot-wire anemometer measurements are presented. A directionally sensitive laser anemometer was used in the separated zone and

Presented as Paper 88-0616 at the AIAA 26th Aerospace Sciences Meeting, Reno, NV, Jan. 11-14, 1988; received May 23, 1988; revision received Feb. 10, 1989.

*Jack E. Cowling Professor, Aerospace and Ocean Engineering Department. Associate Fellow AIAA.
†Visiting Assistant Professor, Aerospace and Ocean Engineering Department.
‡Graduate Research Assistant; presently Research Engineer, Vigyan Research Associates, Hampton, VA.
§Graduate Research Assistant, Aerospace and Ocean Engineering Department.

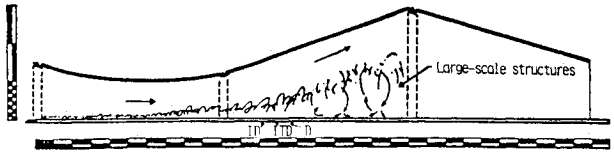

Fig. 1 Sectional schematic diagram of wind tunnel test section. Major divisions on the scales are 0.254 m. Dashed lines show side-wall boundary-layer control-wall jets. Note upper-wall boundary-layer control-wall jets also.

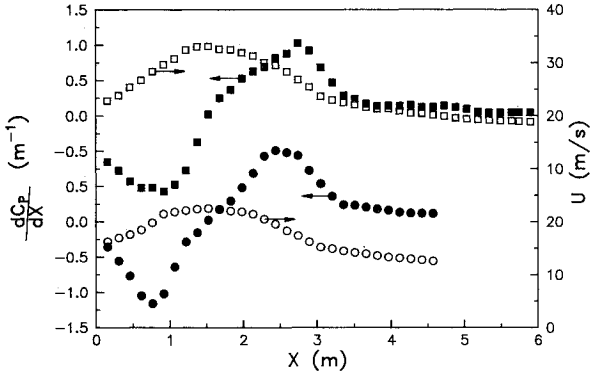

Fig. 2 Pressure gradient distribution and freestream velocity along the tunnel center line for flow without roughness element (flow C; □) and with roughness element (flow D; ○). Note the displaced ordinate. Detachment at 3.71 m.

the region immediately upstream. Data for U, V, $\overline{u^2}$, $\overline{v^2}$, $-\overline{uv}$, γ_{pu} (the fraction of time that the flow moves downstream), streamwise velocity component u power spectra and higher-order turbulent quantities such as $\overline{u^3}$, $\overline{u^4}$, $\overline{v^3}$, and $\overline{v^4}$ are presented in Ref. 3. The flow direction intermittency γ_{pu} was also measured using a thermal tuft.

One purpose for studying these flows is to obtain data at higher Reynolds numbers at detachment ($Re_\theta \geqq 2.8 \times 10^4$) than studied by Simpson et al.[4] ($Re_\theta = 16.3 \times 10^4$). Comparisons are made here with the correlations and observations of Simpson.[1] The scaling of these and streamwise velocity fluctuation spectral data from other experiments is examined here. In companion work not reported here, surface pressure fluctuations have been obtained for these flows.

II. Experimental Equipment

The wind-tunnel configuration (Fig. 1) used for this study is the Low-Speed Boundary-Layer Tunnel at Virginia Polytechnic Institute and State University. The equipment used in these experiments are described in detail in Refs. 3 and 4.

III. Description of Test Flows

Two strong adverse pressure gradient steady freestream flows were studied. In flow C, the freestream velocity at the throat of the tunnel test section at $x = 1.62$ m was 33 m/s, which produced a Re_θ of about 2.8×10^4 near detachment. For flow D, a leading-edge single rectangular cross-section roughness element of 12.5 mm high and 10.3 mm wide was placed across the two-dimensional flow, 51 mm downstream of the blunt leading edge of the plywood floor in order to thicken the boundary layer. The freestream velocity at the throat of the tunnel for this flow was 22 m/s which produced a Re_θ of about 2.9×10^4 near detachment. For each case, the flow reattached some distance downstream.

Figure 2 shows the freestream velocity and nondimensional pressure gradient dC_p/dx distribution for both of the flows obtained along the tunnel centerline of the bottom test wall using the single-wire probe. The mean velocity measurements

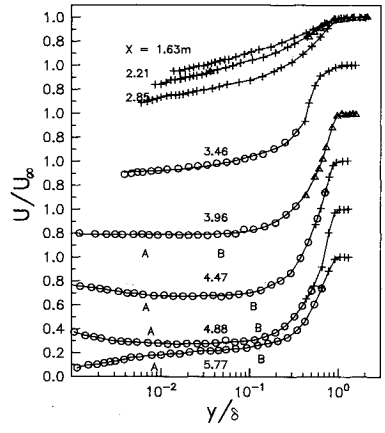

Fig. 3 Nondimensional composite mean-velocity profile from the laser anemometer and hot-wire anemometers for flow C. Note the displaced ordinate for $x > 2.85$ m. Solid lines are for visual aid only. ○ laser; △ cross wire; + single wire.

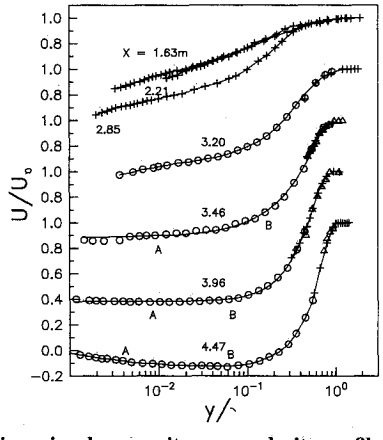

Fig. 4 Nondimensional composite mean-velocity profile from the laser anemometer and hot-wire anemometers for flow C. Note the displaced ordinate for $x > 2.85$ m. Solid lines are for visual aid only. ○ laser; △ cross wire; + single wire.

were repeatable well within the uncertainty of hot-wire anemometer results (±2.4% for the mean velocity). The C_p was calculated using the relation

$$C_p = \frac{2(P - P_i)}{\rho U_{\infty i}^2} = 1 - \left(\frac{U_\infty}{U_{\infty i}}\right)^2 \tag{1}$$

where 'i' denotes freestream entrance condition at a distance of 0.153 m along the tunnel. To determine the derivative of C_p, a five-point local least-square curve fit of C_p data was used at each streamwise location. From Fig. 2 we can observe that the static pressure gradient distribution is similar for both flows. Also, in both of these cases the slope of static pressure gradient changes its sign at about $x = 2.5$ m, where the second wall-jet boundary-layer control unit is located (Fig. 1). Pressure gradient relaxation begins upstream of intermittent transitory detachment near the wall-jet control in these flows and continues weakly downstream of detachment.

IV. Experimental Results and Discussion

A. Mean Velocity Profiles

Mean velocity profiles for both flows are presented in Figs. 3 and 4. Tables 1 and 2 report associated parameters. Upstream of intermittent backflow these composite plots represent hot-wire anemometer measurements. Downstream of intermittent backflow, laser anemometer measurements and valid hot-wire measurements are presented. To check the

Table 1 Parameters of the mean flow development for flow without roughness element (flow C)

x, m	U_∞, m/s	dU_∞/dx, s^{-1}	$\delta_{0.99}$, cm	δ^*, cm	Re_θ	H_{12}	$10_3 \times C_f$	$U_N U_\infty$
1.63	31.47	−1.624	2.2064	0.2549	3958.8	1.2965	3.1708	—
2.21	29.30	−5.533	3.5666	0.4433	5724.7	1.4459	2.4814	—
2.85	24.49	−9.203	5.0800	1.2025	11641.7	1.6250	1.3795	—
3.46	21.23	−2.890	16.3223	5.1079	27587.9	2.5145	0.1161	—
3.96	19.80	−1.724	20.8585	10.6095	36293.1	3.7118	—	0.012
4.47	19.59	−1.556	31.9532	17.0502	40883.0	5.6861	—	0.105
4.88	18.07	−1.551	40.1551	22.3519	43862.8	5.8935	—	0.130
5.77	14.24	−0.588	38.8595	13.5157	54421.5	2.2700	0.1907	—

Table 2 Parameters of the mean flow development for flow with roughness element (flow D)

x, m	U_∞, m/s	dU_∞/dx, s^{-1}	$\delta_{0.99}$, cm	δ^*, cm	Re_θ	H_{12}	$10^3 \times C_f$	$U_N U_\infty$
1.63	21.45	−0.881	2.4600	0.1897	2052.1	1.2619	3.8143	—
2.21	20.33	−5.325	9.4102	0.7428	7808.0	1.2396	2.7956	—
2.85	16.11	−6.041	15.2400	1.6997	11600.2	1.5070	1.4328	—
3.20	14.07	−3.168	16.9370	2.8512	13110.2	1.8895	0.5417	—
3.46	13.60	−2.146	21.4503	6.6817	24351.6	2.4401	0.2071	—
3.96	13.04	−1.594	32.1005	13.1089	29105.7	3.7614	—	0.02
4.47	12.09	−1.221	37.8746	21.7251	31268.8	7.1653	—	0.13

validity of hot-wire measurements from the region of flow reversal (where γ_{pu} is less than unity), the following approximations were used as a check. In the case of single-wire data, $u'/U < 0.3$ if the measurements are valid with no signal rectification.[5] For cross-wire data, if the magnitude of the flow incidence angle to the cross-wire bisector is less than or equal to 30 deg, then the data are considered valid, i.e., $\beta = \tan^{-1}|(V + 2v')/(U - 2u')| \leqq 30$ deg. By these criteria the validity of cross-wire and single-wire data decreases in the direction of decreasing γ_{pu}.

Valid hot-wire data for the mean velocity show good agreement within 3% with laser measurements with an overlap region, thus demonstrating the reliability of measurements by different techniques. The laser-anemometer results obtained on different days at the same location indicated a same level of data repeatability. The uncertainties in laser-anemometer measurements at 20 : 1 odds are as follows: mean velocity $(U) \pm 0.1$ m/s; $\overline{u^2} \pm 3\%$ of maximum profile value; $\gamma_{pu} \pm 0.02$; and $-\overline{uv} \pm 5\%$ of maximum profile value. Uncertainties for hot-wire anemometer measurements are as follows: $\overline{u^2} \pm 7\%$ for the single wire; $\overline{u^2} \pm 10\%$, $-\overline{uv} \pm 15\%$ for the cross wire.

For attached flow upstream of any flow reversal, the law-of-the-wall velocity profile holds. The extent of the semilogarithmic region for the law of the wall decreases continuously after the beginning of intermittent flow reversal. The mean wall shear stress values (Tables 1 and 2) upstream of intermittent detachment were obtained by the Coles and Hirst[6] method, which is based on the law of the wall and requires that for a given U_τ, $U^+ = 16.23$ at $y^+ = 100$. Close to detachment, C_f values obtained by the Coles and Hirst method are 6% lower than values obtained by the Ludwieg-Tillmann[7] skin-friction relation. This difference reduces to as little as 1.2% far upstream of intermittent backflow.

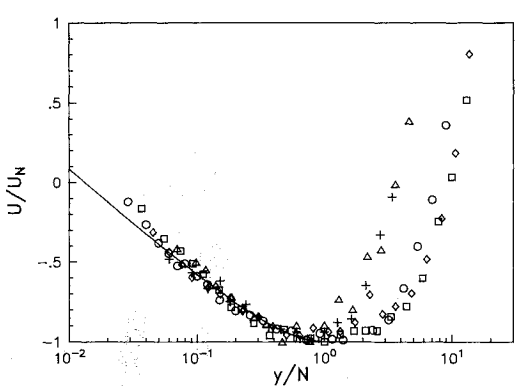

Fig. 5 Normalized backflow mean velocity profiles. U/U_N vs y/N. flow C: +3.96 m; □ 4.47 m; ◇ 4.88 m. flow D: △ 3.96 m; ○ 4.47 m. Solid line represents Eq. (2) with $A = 0.3$.

In the inner region where the backflow exists, the law of the wall for attached flow does not hold. Both of these flows exhibit profile similarity in the backflow region as shown in Figs. 3 and 4. To get a better understanding of this similarity in the backflow region, U and y are normalized with the maximum negative velocity $|U_N|$ and its distance N from the wall, respectively, as shown in Fig. 5. The solid line in this figure is a semi-empirical relation[8] for $0.02 < y/N < 1.0$:

$$\frac{U}{|U_N|} = A\left[\frac{y}{N} - \ell n\left(\frac{y}{N}\right) - 1\right] - 1 \tag{2}$$

based on a semilogarithmic overlap region between the viscous wall layer and the large-scaled outer region. This correlation of negative velocity agrees with the data of other researchers[8] with $A = 0.3$. Dianat and Castro[9] obtained $A = 0.235$ for their separating boundary layer. Even though there is some scatter in the present data and the Simpson et al.[4] data, Eq. (2) with $A = 0.3$ gives a better fit than with $A = 0.235$. Thus, it seems that there exists a "universal law" for negative velocity correlation given by Eq. (2), although there is some question on a unique value of the constant A. The law-of-the-wall velocity profile is not consistent with this correlation, since the law-of-the-wall length scale ν/U_τ varies inversely with its velocity scale U_τ, whereas U_N and N both increase in the direction of decreasing γ_{pu}.[8]

The maximum negative velocity U_N varies with H for detaching flow data[10] by

$$\frac{|U_N|}{U_\infty} = 0.807\left(1 - \frac{1}{H}\right) - 0.577 \tag{3}$$

Simpson[1] found that the data of other investigators for adverse-pressure-gradient-induced separation agreed with this equation. The reattaching flow data[1] from several investiga-

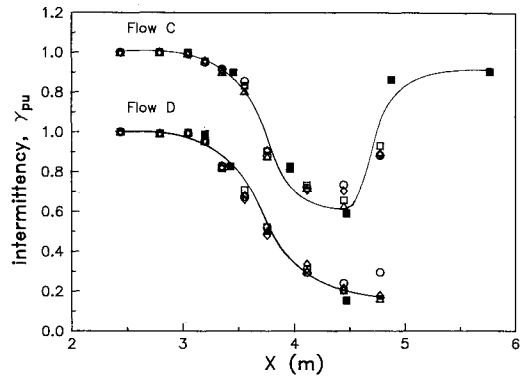

Fig. 6 Fraction of time that the flow is in downstream direction at 1.2. mm from the wall vs x for flows C and D. Solid line is for visual aid only. ■ laser; ○, □, △, ◇ thermal tuft for two ordination.

tors is approximated by:

$$\frac{|U_N|}{U_\infty} = \frac{4}{3}\left(1 - \frac{1}{H}\right) - 1 \tag{4}$$

The present detaching flow data support these general observations although they show higher values compared to Eqs. (3) and (4).

B. Downstream-Upstream Intermittency

The fraction of time that the flow moves in the downstream direction, γ_{pu}, was obtained by laser Doppler velocimeter measurements. The γ_{pu} vs. x at 1.2 mm from the floor was measured also by a thermal tuft and is presented in Fig. 6 with LDV results at the same location. The tuft data were obtained at 0 and 180 deg orientations of the tuft at each x location. In each orientation one sensor wire detects forward flow over the central heater wire while the other sensor wire detects backward flow. Two sets of data were obtained using the thermal tuft in each orientation. All of these measurements show a good agreement with a maximum discrepancy of 7%.

In flow C, ID occurs at 3.05 m, ITD occurs at 3.46 m, and TD and D occur at 3.71 m from the leading edge. This flow reattaches at $\gamma_{pu} = 0.5$ (at 1.2 mm from the wall), which is approximately at 4.7 m from the leading edge. In the flow D, ID occurs at 3.05 m, ITD occurs at 3.36 m, and TD and D occur at 3.71 m from the leading edge. The locations of ITD and D are close to the locations of "intermittent separation" and "fully developed separation," respectively, as defined by Sandborn and Kline (Fig. 4a of Ref. 11), based on H and $\delta^*/\delta_{0.99}$ from mean velocity profiles.

The γ_{pu} vs y distributions reach a minimum value $\gamma_{pu\,\min}$ near the wall downstream of ITD and show some $(\gamma_{pu} - \gamma_{pu\,\min})/(1 - \gamma_{pu\,\min})$ vs y/M similarity[3], where M is the distance from the wall to the location of the maximum $-\overline{uv}$ value. Data for $\gamma_{pu} < 0.8$ at 1.2 mm from the wall correlate together, and data for $0.8 < \gamma_{pu} < 1.0$ at 1.2 mm from the wall correlate together, which is consistent with results from the Simpson et al.[4] flow.

C. Turbulence Quantities

Plots of u'/U_∞ vs y/δ are shown in Figs. 7 and 8. To minimize the uncertainty in cross-wire probe data in the separated region, measurements were performed with the probe axis oriented parallel to the test wall in the attached flow region and parallel to the top wall of the tunnel in the separated region. After the measurements, all of the data were rotated into a test wall coordinate system. Measurements of turbulence quantities by the cross wire show good agreement with single-wire (u' only) and LDV measurements with less discrepancy than the uncertainties of these measurements.

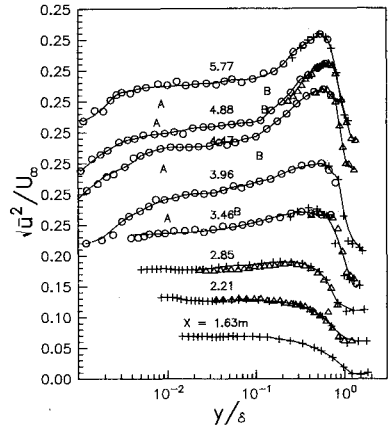

Fig. 7 Axial turbulence intensity profiles, $\sqrt{u^2}/U_\infty$ vs y/δ for flow C. Note the displaced ordinate. Solid lines are for visual aid only. ○ laser; △ cross wire; + single wire.

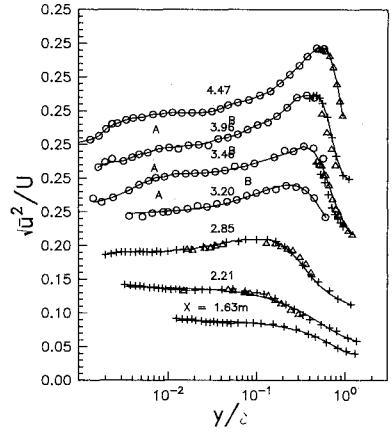

Fig. 8 Axial turbulence intensity profiles, $\sqrt{u^2}/U_\infty$ vs y/δ for flow C. Note the displaced ordinate. Solid lines are for visual aid only. ○ laser; △ cross-wire; + single-wire.

Near the wall $\overline{u^2}$ is greater than $\overline{v^2}$ at all the locations[3] as observed by Simpson et al.[4] From incipient detachment ($x = 3.05$ m) downstream, the slope of u'/U_∞ first increases with $\log(y/\delta)$ and then decreases to a constant value at location "A" over a short region ($0.01 < y/\delta < 0.1$) before increasing again at location "B" until reaching a maximum value in the flow. In their separated flow work, Shiloh et al.[12] have also reported a semilogarithmic region in the range $0.01 < y/\delta < 0.1$. The γ_{pu} remains low until the location "B" where it starts increasing dramatically. In this region $\partial U/\partial y$ is also small, as seen in Figs. 3 and 4.

This semilogarithmic region in the u' profile may be due to two different sets of scaling parameters dominating the inner and outer region of the flow. In the inner region the turbulent motion for u' may be represented as

$$u'/U_\infty = f\left(\frac{y}{y_w}\right) \tag{5}$$

where U_w and y_w are wall region scaling parameters. Here y_w has to be some function of viscosity. In the outer region the scaling parameters can be U_∞ and δ such that

$$u'/U_\infty = g\left(\frac{y}{\delta}\right) \tag{6}$$

If so, then the overlapping region should satisfy these two relations simultaneously. The only function that matches two

different length scales is logarithmic.[13] However, the slope of the semilogarithmic region in each profile was found to be different in the present study and also in Ref. (12). Various scaling parameters have been tried to correlate this longitudinal fluctuating velocity component. The parameters involved were M, N, δ, $-\overline{uv}_{max}$, u'_{max}, v'_{max}, and $\partial U/\partial y|_{max}$. However, none of the attempts showed any satisfactory correlation of the semilogarithmic u' profiles.

The maximum value of u^2 along the streamwise direction was noted to increase until the flow reattaches after separation. Once the flow is reattached, the maximum value of u^2 decreases. The normal and Reynolds shear stress components v^2 and $-\overline{uv}$ maximum values increased even after the flow reattachment. All of these three turbulent quantities show profile similarity and low levels of Reynolds shearing stress in the wall region after detachment.[3]

D. Turbulent Shear Stress Correlation

The distribution of shear stress correlation coefficient $-\overline{uv}/u'v'$ is a measure of the correlation between u and v fluctuations and is largest near the maximum shear stress location in each profile. Upstream of detachment, the correlation coefficient is nearly independent of y in the inner half of the boundary layer.[1,3] This constant value was about 0.42 at $x = 2.2$ m and monotonically decreases to as low as 0.3 in the vicinity of the beginning of intermittent backflow. This is consistent with the Schubauer and Klebanoff[13] shear stress correlation coefficient distribution in their strong adverse pressure gradient boundary-layer flow, even though the adverse-pressure gradient distributions are different.

Unlike the distribution far upstream, the shear stress correlation coefficient does not exhibit a constant value over a large part of the outer layer once the backflow starts to appear. As one moves downstream, the peaks of the distribution seem to move gradually toward the outer edge of the shear layer with a maximum correlation coefficient of 0.3 (Figs. 9 and 10). Once the flow starts reattaching, the correlation coefficient increases to a higher maximum value of 0.4 again.

All of these observations are in agreement with those of Simpson et al.[4] for a similar adverse pressure gradient distribution. Upstream of intermittent backflow, the maximum value in a shear stress correlation coefficient profile noted by them was as high as 0.5 and decreased downstream. In the backflow region, the maximum profile correlation coefficient of about 0.3 was observed in Fig. 13 of Ref. 4.

E. Spectral Measurements

Spectra describe the energy distribution among different sizes of eddies, i.e., largest eddies to the smallest eddies where energy is dissipated. Based on dimensional analysis Perry et al.[14] have proposed a scaling for the power spectrum in an attached flow turbulent wall region (defined as $yU_\tau/\nu \gg 1$ and $y/\delta < 1$). They define three types of scaling: inner, outer, and Kolmogoroff or dissipating eddy. Many researchers have used inner flow scaling, showing good agreement in zero and favorable pressure gradient flows.[15,16] The only adverse pressure gradient flow power spectral studies available in the literature were those of Refs. 17–19. However, none of these studies examined the effectiveness of the inner scaling for adverse pressure gradient flow conditions.

In this study an attempt has been made to check the validity of the Perry et al.[14] inner flow scaling under adverse pressure gradient conditions. It is known that in the detached and near-detached flow regions U_τ is nearly zero, and the maximum shearing stress controls the flow behavior.[1] Upstream of the adverse pressure gradient region the maximum local Reynolds shearing stress is equal to the wall shear stress. Thus, in adapting the Perry et al.[14] scaling for the present study, the maximum Reynolds shear stress is used as a scaling parameter instead of τ_w. The model equations proposed[14] in terms of inner flow scaling with the maximum Reynolds shear stress instead of τ_w are as follows:

$$\frac{\phi_{uu}(k_1 y)}{-uv_{max}} = \frac{A_0}{k_1 y} \tag{7}$$

for the k_1^{-1} spectral region (present only in the near-wall "law-of-the-wall" zone of attached flow),

$$\frac{\phi_{uu}(k_1 y)}{-uv_{max}} = \frac{K_0}{\kappa^{\frac{2}{3}}(k_1 y)^{\frac{5}{3}}} \tag{8}$$

for the $k_1^{-5/3}$ inertial subrange spectral region,

$$\frac{\phi_{uu}(k_1 y)}{-uv_{max}} = \frac{1y^{+4}}{126(k_1 y)^7} \tag{9}$$

for the k_1^{-7} dissipating eddy spectral region. Here, $A_0 = 0.833$, $K_0 = 0.49$, and $\kappa = 0.41$, which are universal constants.

In flows C and D, u power spectra were taken at five different streamwise locations. Spectral data were obtained only at y locations where $\gamma_{pu} = 1$ using the single hot-wire probe. Near the wall upstream of incipient detachment, spectral measurements show excellent agreement with the model equation (7) with a k_1^{-1} law region (Ref. 3, Figs. 25 and 26). Farther from the wall and downstream, but upstream of the beginning of intermittent backflow, a $k_1^{-5/3}$ law region starts dominating the higher wavenumber energy structure. These spectra do not fall on top of one another in inner variables scaling, although a k_1^{-1} envelope bounds the top of each spectrum (Ref. 3, Figs. 25–28). This kind of envelope was also reported by Perry et al.[20] and Ahn[15] in their zero and favorable pressure gradient flows. Since the flow is attached in this region, the spectral scaling exhibits the wall-bounded flow

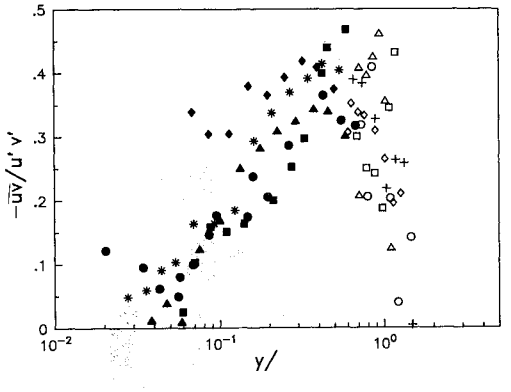

Fig. 9 Distribution of shear stress correlation coefficient, $-\overline{uv}/u'v'$ vs y/δ for flow C. Solid symbols for laser and open symbols for cross-wire data. □ 3.45 m; ○ 3.96 m; △ 4.47 m; ◇ 4.88 m; + * 5.77 m.

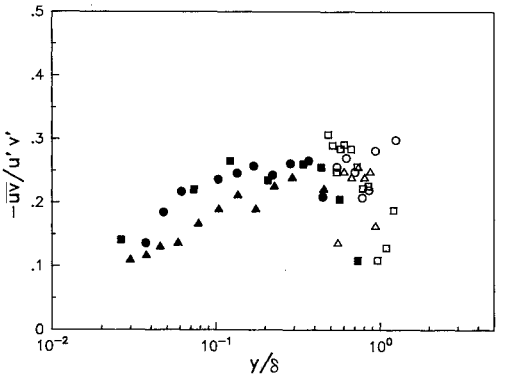

Fig. 10 Distribution of shear stress correlation coefficient, $-\overline{uv}/u'v'$ vs y/δ for flow D. Solid symbols for laser and open symbols for cross-wire data. □ 3.45 m; ○ 3.96 m; △ 4.47 m.

behavior even in the adverse pressure gradient conditions. At streamwise locations with intermittent backflow, the model equations using inner flow scaling fail to show full agreement. No such significant envelope in the spectral distribution was observed as seen upstream of backflow (Ref. 3, Figs. 29 and 30).

In order to get a better correlation of u power spectra downstream of incipient detachment several other scaling parameters have been tried. They involved using the local shear stress at each y location or using the maximum shear stress at a given x location for all y locations. In another attempt the normal stresses turbulence energy production was considered, since it is significant in detaching flows. The ratio of total turbulence energy production to the shear stress turbulence energy production was multiplied by the local shearing stress to obtain a candidate scaling stress.

From all of these attempts, only the outer flow variable δ instead of the inner flow variable y shows a good correlation at all streamwise locations whether attached or detached. The inverse power law and $-5/3$ law with δ as scaling parameter are for the k_1^{-1} region,

$$\frac{\phi_{uu}(k_1\delta)}{-uv_{\max}} = \frac{A_2}{k_1\delta} \tag{10}$$

and for the $k^{-5/3}$ region.

$$\frac{\phi_{uu}(k_1\delta)}{-uv_{\max}} = \frac{K_2}{(k_1\delta)^{\frac{5}{3}}} \tag{11}$$

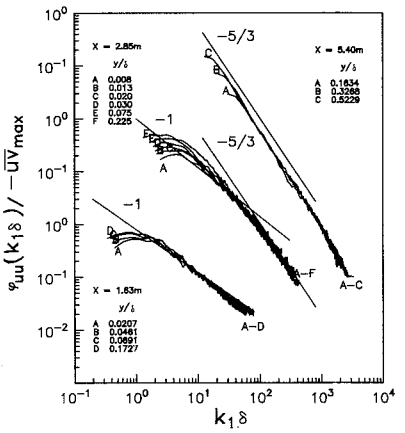

Fig. 11 Normalized u' power spectral distribution from single-wire measurements for flow C. Note the displaced ordinate. Solid lines represent Eqs. (12) and (13).

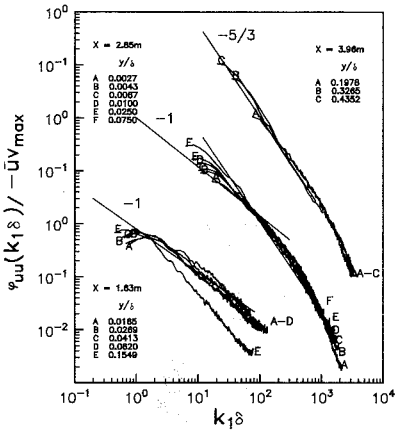

Fig. 12 Normalized u' power spectral distribution from single-wire measurements for flow D. Note the displaced ordinate. Solid lines represent Eqs. (12) and (13).

Upstream of intermittent backflow, Fig. 11 (at $x = 1.63$ m) shows a good correlation of spectral data that agrees with the model equation (10) representing the inverse power law. The outer flow scaling does not show any envelope in the spectral distribution as observed with the inner flow scaling. In this type of scaling, the constant A_2 of the model equation (10) is still 0.833 as for Eq. (7). Thus, the type of scaling using either inner or outer flow parameters does not have any significant effect on the spectral distribution in unseparated flows. For outer-flow scaling, the inverse power law region appears in the wavenumber range of $k_1\delta \simeq 1$ deg $\sim 4 \times 10^1$ where $\phi_{uu}(k_1\delta)/-\overline{uv}_{\max}$ ranges from $4 \times 10^{-2} \sim 5 \times 10^{-1}$.

In the strong adverse pressure gradient and detached flow region (after 2.85 m for both flows), the inverse power law loses its significance and a dominant $-5/3$ spectral region with a good correlation can be noted when outer flow variables are used. The constant K_2 of the model equation (11) for the $-5/3$ region has a higher value for outer flow scaling than K_0. The $-5/3$ law with $K_2 = 20.84$ presents a best fit to this type of scaling for the adverse pressure gradient flows, although at a given x location the spectra seem to collapse better with slightly different values of K_2.

From Figs. 11 and 12 one sees that u power spectra deviate from these power laws at lower wavenumbers. This deviation is greater at lower Reynolds numbers and y/δ at the low wavenumber end. At higher wavenumbers all spectra show a good collapse, reflecting good spatial measurement resolution over the higher frequency inertial subrange. The data match quite well with the $-5/3$ line associated with the higher value of constant $K_2(\simeq 20.84)$ in the inertial subrange. However,

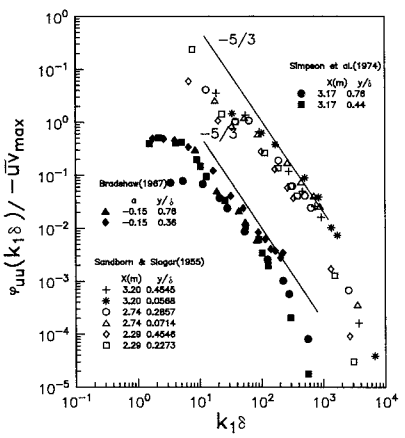

Fig. 13 Normalized u' power spectral distribution for other researchers using Eq. (13). Note the displaced ordinate.

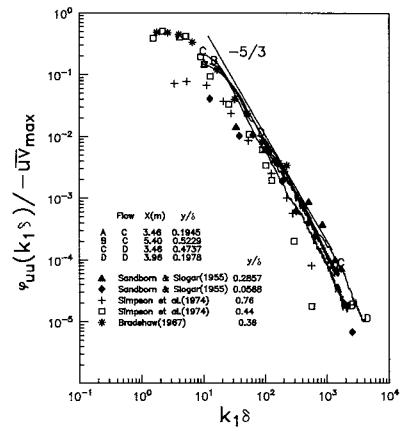

Fig. 14 Normalized u' power spectral distribution with other studies. Solid line represents Eq. (13).

once flow reattachment begins, the spectral data (Fig. 11 at $x = 5.4$ m) do not quite match with the $-5/3$ line associated with $K_\delta^2 = 20.84$. This may be due to the fact that the Reynolds shear stress development lags the u^2 development in reattaching flows. The inertial subrange has almost the same wavenumber range of $k_1\delta \simeq 4 \times 10^1$ to 10^3 with its value ranging from 10^{-4} to 5×10^{-1} for both detached flows.

The present data with the outer flow scaling are compared with results from other adverse pressure gradient studies. The Simpson et al.[17] data for an adverse pressure gradient separated flow, Bradshaw[18] data for an equilibrium attached boundary-layer flow, and the Sandborn and Slogar[19] data for a strong adverse pressure gradient turbulent boundary layer are presented in Fig. 13 with the outer flow scaling parameter δ. Figure 14 shows a good comparison of arbitrarily selected present data with data from these other flows. In the present study the outer flow scaling parameter correlated spectra for $0.5 < u^2/-\overline{uv}_{\max} < 2.8$.

This scaling result implies that the turbulence kinetic energy dissipation rate ε is constant across the flow at a given x location where this relation holds. In other words, since the spectral inertial subrange is described by

$$\phi_{uu}(k_1\delta) = 0.49(\varepsilon\delta)^{\frac{2}{3}}(k_1\delta)k_1^{-5/3} \tag{12}$$

then Eqs. (11) and (12) yield

$$\varepsilon = \left(\frac{20.84}{0.49}\right)^{\frac{3}{2}} \frac{(-\overline{uv}_{\max})^{\frac{3}{2}}}{\delta} \tag{13}$$

which is independent of y over the middle half of the shear layer at a given x location. Simpson et al.[17,21] show that ε is almost constant over the middle of their separated shear flow at a given streamwise location.

V. Conclusions

Since the maximum shearing stress and the shear layer thickness are dominant stress and length scales for detaching and separated flows, it is consistent that streamwise velocity spectra away from the reversed flow zone should scale on these parameters in the $k_1^{-5/3}$ inertial subrange law. This implies that the energy dissipation rate is nearly constant over the region where this scaling holds. The inner-flow length scale of distance from the wall fails to correlate these spectra. Upstream of intermittent backflow in the near-wall region the production of turbulence is still dominant and the spectra for the nonviscous subrange varies with k_1^{-1}.

The mean velocity profile data for the backflow of these flows agree with the proposed model profile of Simpson,[8] which scales on the local maximum negative mean velocity U_N and its distance from the wall N. A semilogarithmic variation of u' from the wall exists in the near wall detaching and detached flow region, although no consistent correlation of the profiles from various data sets was found. For $16.3 \times 10^4 < Re_\theta < 4.7 \times 10^4$ the structure discussed here is Reynolds-number independent.

Acknowledgments

This study was supported by NASA Langley Research Center under Grant 1-466 and by the Air Force Office of Scientific Research under Grant 84-0134. The authors acknowledge the assistance of S. Ahn in this research.

References

[1]Simpson, R. L., "Two-Dimensional Turbulent Separated Flow," AGARDograph Vol. 1, No. 287, June 1985.

[2]Simpson, R. L., "Two-Dimensional Turbulent Separated Flow," *AIAA Journal*, Vol. 25, June 1987, pp. 775–776.

[3]Nagabushana, K. A., Simpson, R. L., and Agarwal, N. K., "Experimental Study of Two Separating Turbulent Boundary Layers," NASA CR-181011, May 1987.

[4]Simpson, R. L., Chew, Y. T., and Shivaprasad, B. G., "The Structure of a Separating Turbulent Boundary Layer. Part I. Mean Flow and Reynolds Stresses," *Journal of Fluid Mechanics*, Vol. 113, 1981, pp. 23–51.

[5]Simpson, R. L., "Interpreting Laser and Hot-Film Anemometer Signals in a Separating Boundary Layer," *AIAA Journal*, Vol. 14, Jan. 1976, pp. 124–126.

[6]Coles, D. and Hirst, E. A., "Computation of Turbulent Boundary Layers," *1968 AFOSR-IFP-Stanford Conference*, Stanford University Press, Stanford, CA, 1969, pp. 48–50.

[7]Ludwieg, H. and Tillmann, W., "Investigation of the Wall-Shearing Stress in Turbulent Boundary Layers," NACA TM-1285, 1950.

[8]Simpson, R. L., "A Model for the Backflow Mean Velocity Profile," *AIAA Journal*, Vol. 21, Jan. 1983, pp. 142–143.

[9]Dianat, M. and Castro, I. P., "Measurements in Separating Boundary Layers Using Pulsed Wire Anemometry," International Council of Aerospace Sciences, Paper ICAS-86-1.7.2, 1986.

[10]Simpson, R. L. and Shivaprasad, B. G., "The Structure of a Separating Turbulent Boundary Layer. Part 5. Frequency Effects on Boundary Layers," *Journal of Fluid Mechanics*, Vol. 29, Pt. 4, 1967, pp. 625–645.

[11]Sandborn, V. A. and Slogar, R. J., "Longitudinal Turbulent Spectrum Survey of Boundary Layer in Adverse Pressure Gradients," NACA TN-3453, 1953.

[12]Shiloh, K., Shivaprasad, B. G., and Simpson, R. L., "Feature of a Separating Turbulent Boundary Layer. Part 3. Transverse Velocity Measurements," *Journal of Fluid Mechanics*, Vol. 113, 1981, pp. 75–90.

[13]Schubauer, G. B. and Klebanoff, P. S., "Investigation of Separation of the Turbulent Boundary Layer," NACA Rept. 1030, 1951, pp. 75–90.

[14]Perry, A. E., Lim, K. L., and Henbest, S. M., "A Spectral Analysis of Smooth Flat-Plate Boundary Layers," *Proceedings of the 5th Symposium on Turbulent Shear Flows*, 1985, Springer-Verlag, New York, pp. 9.29–9.34.

[15]Ahn, S., "Some Unsteady Features of Turbulent Boundary Layers," MS Thesis, Dept. Aerospace and Ocean Engineering, Virginia Polytechnic Institute and State University, Blacksburg, VA, 1986.

[16]Erm, L. P., Smits, A. J., and Joubert, P. N., "Low Reynolds Number Turbulent Boundary Layers on a Smooth Flat Surface in a Zero Pressure Gradient," *Proceedings of the 5th Symposium on Turbulent Shear Flows*, 1985, Springer-Verlag, New York, pp. 2.13–2.18.

[17]Simpson, R. L., Strickland, J. H., and Barr, P. W., "Laser and Hot-Film Anemometer Measurements in a Separating Turbulent Boundary Layer," National Technical Information Service, Rept. AD-A001115, 1974.

[18]Bradshaw, P., "The Turbulence Structure of Equilibrium Boundary Layers," *Journal of Fluid Mechanics*, Vol. 29, Pt 4, 1967, pp. 625–645.

[19]Sandborn, V. A. and Slogar, R. J., "Longitudinal Turbulent Spectrum Survey of Boundary Layer in Adverse Pressure Gradients," NACATN-3453, 1953.

[20]Perry, A. E., Henbest, S. M., and Chong, M. S., "A Theoretical and Experimental Study of Wall Turbulence," *Journal of Fluid Mechanics*, Vol. 165, 1986, pp. 163–199.

[21]Simpson, R. L., Strickland, J. H., and Barr, P. W., "Features of a Separated Turbulent Boundary Layer in the Vicinity of Separations," *Journal of Fluid Mechanics*, Vol. 79, 1977, pp. 553–594.